 

PACS numbers: 42.68.Wt; 42.60.By; 42.65.Re; 42.65.Jx; 42.65.Ky
DOI: 10.1070/QE2014v044n06ABEH015431

# Lidar sensing of the atmosphere with gigawatt laser pulses of femtosecond duration

O.A. Bukin, M.Yu. Babii, S.S. Golik, A.A. Il'in, A.M. Kabanov, A.V. Kolesnikov, Yu.N. Kulchin, V.V. Lisitsa, G.G. Matvienko, V.K. Oshlakov, K.A. Shmirko

*Abstract.* **We present the results of sensing of the atmosphere in the condition of a transition 'continent–ocean' zone by means of gigawatt femtosecond pulses of the fundamental and second harmonics of a Ti:sapphire laser. In the regime of multi-frequency sensing (supercontinuum from the fundamental harmonic) the emission lines of the first positive system of the nitrogen molecule $B^3\Pi_g - A^3\Sigma_u^+$ have been recorded, while the sensing using of the second harmonic have revealed the possibility of detecting the lines of Raman scattering of nitrogen ($\lambda$ = 441 nm). The intensity ratio of the line of Raman scattering of nitrogen and the line of elastic scattering at the wavelength of $\lambda$ = 400 nm amounts to $5.6\times10^{-4}$.**

***Keywords:*** *lidar, multi-frequency sensing, supercontinuum, ultrashort pulses, atmosphere, elastic scattering, Raman scattering, spectrum.*

## 1. Introduction

Presently, the development of lidar sensing of the air and water systems by means of high-power femtosecond systems is carried out in Russia by the research teams of Moscow State University, Far Eastern Federal University, as well as several institutions of RAS, such as Institute of Applied Physics (Nizhnii Novgorod), Institute of Laser Physics SB RAS (Novosibirsk), Institute of Atmospheric Optics SB RAS (Tomsk), Institute of Automation and Control Processes (IACP) FEB RAS (Vladivostok). Each of these institutions possesses a powerful femtosecond giga- and terawatt system in action [1, 2].

Formally, in order to work in this direction, the RAS institutions are jointed together within the project programme 'Extreme Light Fields and Their Applications' of the Presidium of RAS and the integrated project 'Development of Methods for Femtosecond Laser Sensing of The Atmosphere' of SB RAS – FEB RAS. In the framework of these projects, a series of theoretical and experimental studies on the processes of formation of filaments and their characteristics, as well as investigation of the interaction of the filamented pulses with different media [2–6] have been conducted. These studies involve the experiments on atmospheric sensing on short atmospheric paths (Nizhnii Novgorod, Novosibirsk, Tomsk); the first experiments on atmospheric sensing by femtosecond pulses using the effect of filamentation and generation of the supercontinuum on the inclined atmospheric paths (Vladivostok, Tomsk); and accumulation of a database for the analysis and subsequent development of environmental sensing techniques using the high-power femtosecond systems.

A specific feature of remote sensing of the atmosphere with the femtosecond lasers is the use of the radiation from the supercontinuum (SC) – a phenomenon of spectral and spatiotemporal broadening of a high-power ultrashort probing pulse. The SC accompanies the filamentation of the initial pulse: if the pulse power exceeds a certain threshold (about 3.2 GW), a nonlinear addition to the refractive index becomes significant in the interaction region, and a self-focusing regime is observed, which is followed by the process of filamentation and generation of conical SC emission. The SC spectral components are distributed within the cones with a vertex at the point of its generation. The direction of SC radiation coincides with the direction of pulse propagation. The SC radiation is observed both in Stokes (relative to the laser wavelength) and anti-Stokes spectra in the spectral range of several octaves. The total losses of the pulse energy relevant to the filamentation and generation of the conical SC emission do not exceed 20%. Thus, a source of the short-duration pulses in a wide spectral range, with the characteristics close to the laser ones, is formed on the path of sensing.

To solve the direct and inverse problems of atmospheric sensing, and to meet the challenges of the development of new lidar systems, the information is required concerning the typical parameters of the medium through which the filamented ultrashort sensing pulses (USPs) propagate: the attenuation coefficient (linear and nonlinear) both due to scattering and absorption, indicatrix of scattering on atmospheric components, backscattering factor, lidar ratio, variation of the polarisation characteristics, etc. The required information about these parameters can be obtained both in laboratory and field experiments [7–24].

The SC glow has opened new possibilities for measuring the atmospheric parameters by means of the lidar technique. Even the first steps on application of the femtosecond terawatt lidar in the 1990s have shown that the atmospheric sensing by a femtosecond laser source forms an SC source which ensures the sensing up to significant (12–15 km) altitudes [25–28].

**O.A. Bukin, Yu.N. Kulchin, K.A. Shmirko** Institute of Automation and Control Processes, Far Eastern Branch, Russian Academy of Sciences, ul. Radio 5, 690041 Vladivostok, Russia;
**M.Yu. Babii, A.V. Kolesnikov** Far Eastern Federal University, ul. Sukhanova 8, 690091 Vladivostok, Russia;
**S.S. Golik, A.A. Il'in, V.V. Lisitsa** Institute of Automation and Control Processes, Far Eastern Branch, Russian Academy of Sciences, ul. Radio 5, 690041 Vladivostok, Russia; Far Eastern Federal University, ul. Sukhanova 8, 690091 Vladivostok, Russia; e-mail: golik_s@mail.ru;
**A.M. Kabanov, G.G. Matvienko, V.K. Oshlakov** V.E. Zuev Institute of Atmospheric Optics, Siberian Branch, Russian Academy of Sciences, pl. Akad. Zueva 1, 634021 Tomsk, Russia; e-mail: ovk@iao.ru

Received 3 March 2014; revision received 25 March 2014
Kvantovaya Elektronika **44** (6) 563–569 (2014)
Translated by M.A. Monastyrskiy

The prospects of using the SC served as a basis for developing a number of projects, including international ones, and in particular, a mobile version of a femtosecond terawatt Teramobile lidar. As a part of this project, in the last two decades, the modern lidar systems have been developed, great methodical experience has been accumulated, and a wide range of problems of atmospheric optics is now being solved [29].

The specific features of the filamented pulse that is used as a sensing radiation pulse with a broad spectrum have required a revision of the basic specifications for lidar systems, methods of registration of lidar signals, and lidar equation [2, 3, 30, 31]. Theoretically, it is possible to estimate the position of the nonlinear focus with regard to the emission wavelength, the cross section of the collimated beam of radiation, and the relation between its power and critical self-focusing power [32]. The possibility of the remote positioning of the filamentation point, and hence the point of the SC generation, is experimentally and theoretically proved. A variety of filaments can be formed both in the propagation direction and in the cross section of the radiation beam [33–37]. The authors of paper [2] propose a conditional partitioning of the SCP path of sensing into the initial region of nonlinear interaction (self-focusing regime), another region of nonlinear interaction (filamentation regime in the nonlinear focus zone and generation of the SC conical emission, defocusing and self-focusing) and a linear region. The regions of the self-focusing and filamentation should fall into a 'dead' zone of the lidar because here, due to the reduction of the beam cross section, maximal intensities of the high-power USPs are realised, which commonly exceed the limiting values that are allowable for the photodetector systems.

In this paper we discuss the results of sensing of the atmosphere along a sloping atmospheric path in the conditions of the transition 'continent–ocean' zone using the IACP-FEB lidar system.

The experiments are aimed at studying the possibilities of sensing the atmosphere in this zone by means of the femtosecond lidar with gigawatt-power pulses.

## 2. Experimental setup

The scheme of the experimental facility is presented in Fig. 1. The lidar system is based on a Ti:sapphire laser (*1*) (Spitfire XP40F5W, Spectra Physics) with a chirped two-stage power amplification capable of generating 40-fs pulses with the centre wavelength of 800 nm, half-width spectral range of 30 nm, pulse repetition rate up to 1 kHz and average power up to 7 W.

In this configuration of the femtosecond lidar system, fundamental harmonic radiation pulses with the energies up to 7 mJ and the repetition rate of 1 kHz were generated. Laser radiation was directed into the atmosphere with a system of mirrors (*2*) (UFM10R, Thorlabs). To generate the second harmonic, a 300-μm-thick BBO crystal (*3*) was installed between the mirrors, which ensured the average power of 1.2 W at the centre wavelength of 400 nm, the laser pulse repetition rate of 1 kHz, and the initial fundamental harmonic pulse duration of 45 fs. Thus, the power of the sensing pulses exceeded 20 GW for the second harmonic and did not exceed 100 GW for the fundamental harmonic of the Ti:sapphire laser.

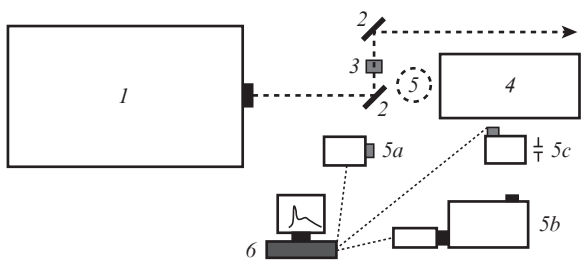


**Figure 1.** Scheme of the experimental facility (see the notations in text).

Spectral dependence of the radiation divergence angle entails the problem of selecting the optimal combination of the lidar system specifications: the system type (coaxial/biaxial), the base (the distance between the optical axes of the transmitting and receiving optical systems), the field of view angle (defined by the relation between the diameter of the field diaphragm and the focal length of the telescope) and its combination with the divergence angles of the SC spectral components, and, finally, the type of the photosensitive receiver.

Taking into account the energy characteristics of the sensing pulse, we preferred the scheme of the biaxial lidar. This guaranteed the exclusion of the signals of nonlinear interactions (self-focusing and filamentation) on the initial parts of the path and ensured the registration of the backscattered signals, including the signal from the linear region at the laser wavelength.

The reception system of the lidar (*4*) is based on the Schmidt–Cassegrain telescope (C11-SGTXLT, Celestron Advanced; the aperture is 279 mm, focal length is 2800 mm, aperture ratio is 1/10). In all experiments, the angle of view of the receiving system did not exceed 1.5 mrad. The telescope and the last rotating mirror that transmitted the probe radiation into the atmosphere were placed on a single platform. The lidar base was 23 cm. The lidar adjustment was performed by varying the angle between the optical axes of the receiving–transmitting system and the angle of sensing with respect to the horizon (oblique sensing). The sensing of the atmosphere was conducted through the laboratory building window with changing the sensing angle from zero (horizon) to 45°.

The equipment of the recording system (*5*) was varied depending on the task to be solved. In the first modification (*5a*) a photomultiplier (R7400U, Hamamatsu) was used as registrar that was matched with the telescope by means of the optical fibre of 1 mm diameter, herewith the removable bandpass interference filters (FKB-VIS-10, Thorlabs) were installed in front of the optical fibre to provide the reception of the signals in the wavelength regions of 445–455 nm, 495–505 nm, 545–555 nm, 595–605 nm, 645–655 nm, 695–705 nm, 745–755 nm and 795–805 nm (depending on the filter). The signal from the photomultiplier was recorded with the use of a high-speed ADC (ADM216×100M (16 bit, 100 MHz) of the JSC 'Instrumental Systems'), combined with a personal computer (*6*).

In the second modification, the registration system (*5b*) consisted of a polychromator (Spectra Pro 2300i, Princeton Instruments; diffraction gratings of 1200, 600, and 300 lines $mm^{-1}$) matched to the telescope by the optical fibre (the entrance from the telescope side was of circular shape with a diameter of 1 mm, while from the monochromator side it represented a slot of $1 \times 0.16$ mm in size), and an ICCD camera (PI-MAX3: 1024i, Princeton Instruments).

In the third modification (*5c*), the registration system involved the field diaphragm, polychromator (77480, Newport; diffraction grating of 300 lines $mm^{-1}$, the entrance slit width

of 1 mm), the 16-channel PMT (H10515B-04, Hamamatsu) and the high-speed ADC (ADM216×100M, JSC 'Instrumental Systems').

For correct estimation of molecular scattering, the data of upper-air sounding have been used [38], which was carried out at a distance of 5 km from the station of sensing. To facilitate the analysis of the results of lidar sensing of the atmosphere, the so-called attenuated scattering ratio was introduced and used by the analogy with [39]:

$$R(z) = \frac{\beta_a(z) + \beta_m(z)}{\beta_m} \exp\left[-2\int_0^z \alpha_a(z)\,dz\right] = \frac{P(z)}{P_m(z)}, \qquad (1)$$

where $z$ is the distance to the area of sensing; $\beta_a(z)$ and $\beta_m(z)$ are the inverse coefficients of the aerosol and molecular scattering, respectively; $\alpha_a(z)$ is the aerosol extinction coefficient; and $P(z)$ and $P_m(z)$ represent the lidar signals caused by the actual and molecular atmosphere, respectively. The value $R(z)$ shows how many times the total lidar signal exceeds the signal which is due to the molecular atmosphere only. On the one hand, this value characterises the aerosol state of the atmosphere, while on the other it characterises the quality of the lidar system adjustment: $R(z) \to 1$ in the area free from the aerosol particles [39, 40].

## 3. Certification of the sensing path

First of all, consider the results of the experiment to determine the distance to the initial region of the atmosphere from which the signals of the backscattered femtosecond sensing pulse can be recorded. This experiment is important in connection with the specific use of the high-power femtosecond pulse as a probe.

As noted above, a powerful ultrashort pulse that propagates in the air becomes self-focused, and the conditions are realised for the SC filamentation and generation. After the 'excess' energy of the pulse has been spent, the nonlinear processes are not observed; in other words, starting from a certain distance, the interaction with the medium of propagation in the entire spectral range of the SC radiation, including the laser wavelength, becomes linear. Consequently, it is necessary to determine the position of the starting point on the path of sensing. In the experiments discussed in this paper, we used the results of preliminary laboratory experiments aimed at determining the position of the point (region) of filamentation on the horizontal propagation path of a gigawatt pulse, depending on the system of the configuration of the mirrors (Fig. 1). Under laboratory conditions, the position of the filamentation point was registered at a distance of 5–10 m from the output mirror (*2*) with the following laser radiation parameters: the centre wavelength of 800 nm, the pulse energy of 6 mJ, the pulse duration of about 50 fs, the beam diameter of 5 mm. The position of the point of the SC generation under the atmospheric conditions was limited to the distance of 5–75 m from the output mirror of the lidar. The instability of the SC generation point is explained by the conditions of the natural experiment, which were different from the laboratory conditions: the sensing of the atmosphere was conducted in the direction of the natural marine waters, usually with the varying temperature and moisture content, which resulted in a change in the conditions of the SCP interaction with the medium of propagation, and, in particular, increased the probability of multiple filamentation.

Spatial redistribution of the spectral energy occurs within a cone with a vertex at the point of filamentation according to the following rule: the shorter the wavelength, the larger the angle at the cone vertex [33]. Previously we obtained the angular dependence of the spectral components for the filamented femtosecond pulses with the energy of 10–40 mJ and the duration of 45–50 fs (at a sub-terawatt power) under self-focusing conditions [24]: the SC radiation was registered in the range of 300–1100 nm and the diameters of the 'spectral' rings of the SC conical emission were determined (for the wavelength $\lambda_{SC}$ = 400 nm, the half-angle of divergence amounted to $4\times10^{-3}$ rad, for $\lambda_{SC}$ = 700 nm – to $5\times10^{-4}$ rad, for $\lambda_{SC}$ = 1100 nm – to $1.2\times10^{-4}$ rad).

As to this paper, in the experiments on sensing the atmosphere in the transition 'continent–ocean' zone, the following method for determining the starting point of sensing was used (the sensing was carried out at the fundamental harmonic wavelength of 800 nm at a pulse duration of 50 fs, energy of 5 mJ and initial beam diameter of 5 mm). The energy and duration of the pulse, as well as the initial cross section of the beam ensured the implementation of nonlinear processes, SC filamentation and generation. The backscattered signals were registered in the spectral interval centred at wavelengths $\lambda$ = 793, 775, 757, 739 and 721 nm [the third modification (*5c*) of the recording system was used, see Fig. 1]. The wavelength of 793 nm was selected as the nearest (according to the upper allowable limit for the input flows of radiation for the given registration system) to the laser wavelength of 800 nm. The signal acquisition time for the intervals with $\lambda$ = 793 and 775 nm was 20 min, for the rest of intervals – 40 min. The dependences $F(z,\lambda) = P(z,\lambda)/P(z,\lambda = 793\text{ nm})$ were determined. When self-focusing and generation of broadband conical emission occur along the propagation path of laser radiation, these nonlinear effects, manifesting themselves in the ring structure of the spectral redistribution of energy, should entail the increase/decrease in the function $F(z,\lambda)$. If the nonlinear effects do not arise, the dependences $F(z,\lambda)$ for a given $\lambda$ will be parallel to each other. Figure 2 represents the dependences $F(z,\lambda)$ obtained by sensing the atmosphere in the transition 'continent–ocean' zone and their approximations. The zenith angle on the path of sensing was 45°. It follows from Fig. 2 that the distance to the region of the atmosphere, the backscattered signal from which fully came into the view of the

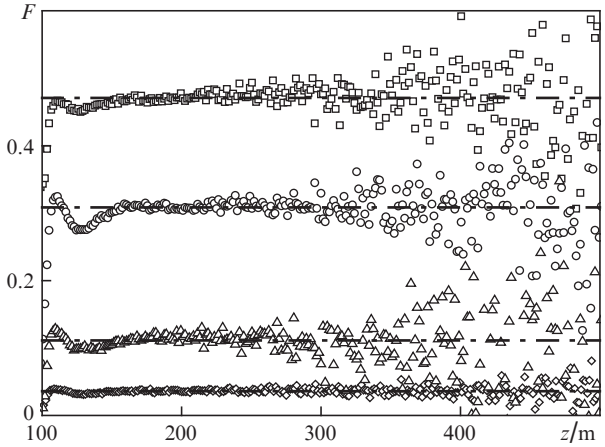


**Figure 2.** Dependences $F(z,\lambda)$ obtained by sensing the atmosphere in the transition continent–ocean zone (November 2013) for $\lambda$ = 775 (□), 757 (○), 739 (△) and 721 nm (◇), and their approximations (dot-dashed lines).

receiving system, amounts to 140 m. It is also seen that radiation propagation on the distances that exceed 140 m for these sensing wavelengths is carried out in the linear regime, which means that the self-focusing and filamentation of radiation occur at distances lesser than this value. The results of such experiments make a basis for the confirmation of the linear nature of femtosecond pulse propagation in the 'post-filamentation' regime.

## 4. Simultaneous sensing by femtosecond (at the wavelength of the second harmonic of laser radiation) and nanosecond lidars

In January 2014, an experiment was conducted on the joint lidar sensing of the night-time atmosphere by the laser pulses of femto- (femtosecond lidar) and nanosecond (nanosecond lidar) durations for the purpose of qualitative comparison of the results. In the case of the femtosecond lidar, the second harmonic of laser radiation ($\lambda = 400$ nm) and the third modification of the recording system [(*5c*) in Fig. 1] were employed. As a nanosecond lidar, we used the multi-frequency lidar IACP FEB RAS [40, 41]. Figure 3 shows the vertical profiles of the attenuated scattering ratio $R(z)$ for the cases of sensing pulses of nano- ($\lambda = 355$ nm) and femtosecond ($\lambda = 400$ nm) duration. It is seen that the dependences $R(z)$ for these two cases are almost identical. The slight differences are due to the differences in the configurations of the receiving and transmitting systems, as well as are caused by the spectral dependence of the coefficients of backscattering and extinction for molecular and aerosol components of the atmosphere which also affect the $R(z)$ ratio.

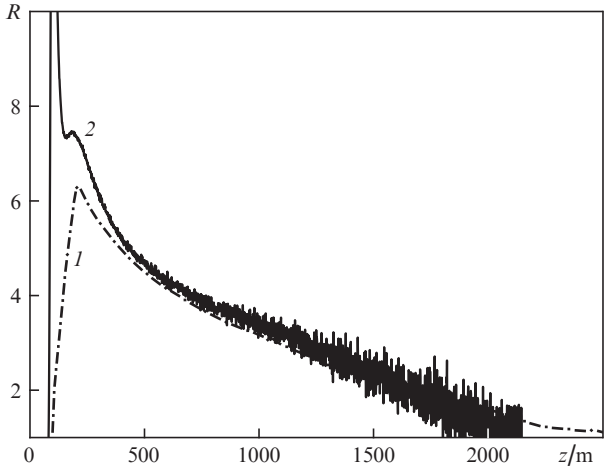


**Figure 3.** Vertical profiles of $R(z)$ for laser radiation pulses of nano- (*1*) and femtosecond (*2*) durations.

## 5. Lidar of elastic scattering

The signal of elastic backscattering of the fundamental harmonic of the Ti:sapphire laser ($\lambda = 800$ nm) was recorded by using the first modification of the recording system [(*5a*) in Fig. 1] (the filter bandpass was 795–805 nm). The laser pulse energy was 6 mJ, its duration was 45 fs, and the beam diameter was 10 mm. The height of full entering of laser radiation into the field of view of the receiving system was 900 m which was consistent with the calculations (about 800 m) [39]. The sensing was conducted on an inclined path at the zenith angle of 65°, the signal acquisition time was 20 min at the repetition frequency of 1 kHz. Figure 4 shows the vertical profiles of the attenuated scattering ratio $R(z)$. The signal/noise ratio for the signals from the initial portions of the path is much greater than unity and decreases down to 1.5 when the area of sensing is 11 km away from the lidar. The application of classical calculation schemes [2] together with the filtering and smoothing algorithms [39] provides a reliable reconstruction of the aerosol backscattering coefficients with an error not exceeding 15%.

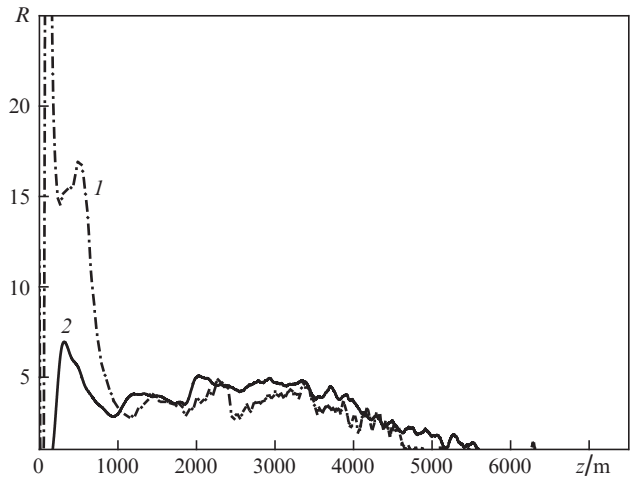


**Figure 4.** Vertical profiles of $R(z)$ obtained when receiving a signal from the near (*1*) and far (*2*) zones. The laser wavelength is 800 nm, and the zenith angle is 65°.

Figure 4 clearly demonstrates the internal structure of the planetary boundary layer up to its boundary at the height of 4000 m, where the signal of aerosol scattering begins to decrease down to the value corresponding to molecular scattering. Variation of the parameters of the lidar adjustment in order to correctly receive the signal from the near-field zone does not significantly change the shape of the backscattering signal; we only deal with a change in the distance to the region of the atmosphere from which the backscattered radiation falls entirely within the field of view of the receiving system.

Taking into account the modern scope of application of the aerosol lidar, which is based on its capability of determining the type and height of the scattering layer (cloud or aerosol), the coefficients of aerosol extinction or backscattering, the vertical extent of the layer, the structure and dynamics of the planetary boundary layer [40, 41], as well as the experimental results described in this section, we distinctly see the prospects of the application of this lidar for studying such structural elements of the troposphere, as the planetary boundary and aerosol layers.

## 6. Multifrequency sensing

To investigate the effectiveness of reconstruction of the atmospheric gas composition in the transition 'continent–ocean' zone using the technique of the multifrequency lidar sensing by means of ultrashort laser pulses, the backscattering spectra obtained in these experiments were analysed for the presence

of emission lines of the gas composition of the atmosphere, as well as for the presence of the Raman lines of atmospheric gases.

This experiment employed a system of registration with a wideband signal gating [(*5b*) in Fig. 1] by varying the delay of the signal registration by the ICCD camera. The recording of the first (in time) spectrum corresponds to the distance of 75 m from the detector, and the time delay for each subsequent recording of the spectrum corresponds to the distance of 28.5 m.

Figure 5 shows the spectra of the backscattered signal received from different parts of the atmospheric path (the 'decimated' spectra are shown for clarity). The laser pulse energy was 6 mJ, its duration – 45 fs, and the beam diameter – 10 mm. It is seen from Figs 5b and 5c that the narrow lines can be distinguished in the spectra obtained against the SC background (broadband continuous radiation) at the wavelengths of 752, 760, 775, 815 and 847 nm, which have much lower intensities than the intensity of the main laser pulse.

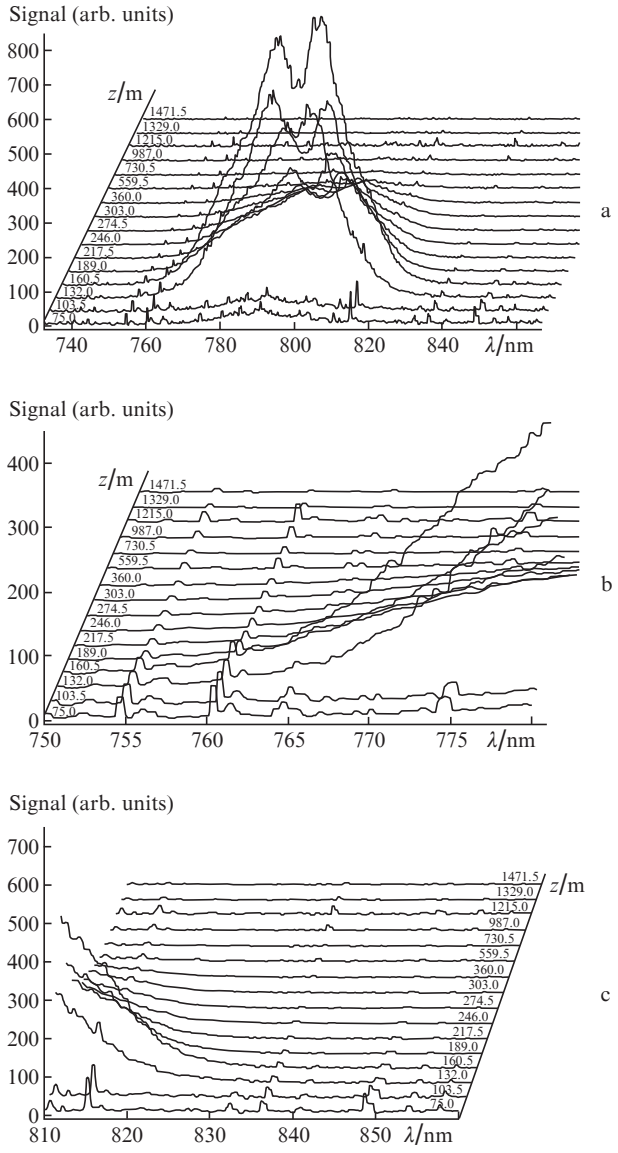


**Figure 5.** Spectrum of the backscattered signal (a) and its anti-Stokes (b) and Stokes (c) regions.

According to our estimates, these lines correspond to the first positive system of the nitrogen molecule $B^3\Pi_g - A^3\Sigma_u^+$. It is interesting to note that we have earlier recorded similar spectra in the observation of the optical breakdown on the surface of the sea water under the action of femtosecond laser pulses [42, 43].

## 7. Reconstruction of the profile of the aerosol extinction coefficient

Figure 6 shows an example of the reconstruction of the profiles of the aerosol extinction coefficients $\alpha_a$ for the laser wavelength 800 nm and for wavelengths 780 and 830 nm (sample spectrograms of the SC lidar signals). The reconstruction has been carried out according to the Klett method with regard to the location of the filamentation point on the sensing path [2]. A 'corridor' of values $\alpha_a \pm 3\sigma$ is indicated for the laser wavelength. It is seen from the comparison of the dependences shown in Fig. 6 that the aerosol extinction coefficients for the close wavelengths (780 and 800 nm) are practically identical. Starting from the height of about 700 m, the extinction coefficient for the wavelength of 830 nm (close to the wavelength of the absorption line $H_2O$) is almost identical to that of the wavelength of 800 nm, which, according to the data of lidar elastic scattering, corresponds to the estimate of the bed height haze.

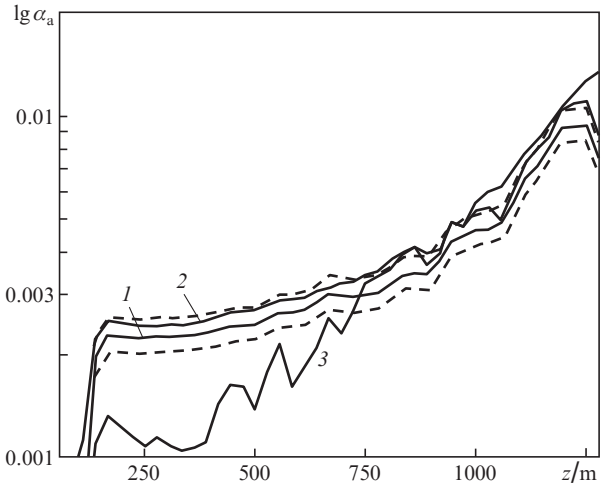


**Figure 6.** Vertical profiles of the aerosol extinction coefficient $\alpha_a$ (in $m^{-1}$) for the wavelengths of (*1*) 800, (*2*) 780 and (*3*) 830 nm. Dashed curves show the profiles $\alpha_a + 3\sigma$ for the wavelength of 800 nm.

## 8. Registration of the Raman scattering signals of nitrogen

To investigate the possibilities of the Raman lidar using the femtosecond laser pulses with a centre wavelength of 400 nm, a 300-μm-thick BBO crystal [(*3*) in Fig. 1] was installed between the mirrors [(*2*) in Fig. 1]. As a result, radiation was obtained at the centre wavelength of 400 nm with the spectral half-width of about 5 nm, the pulse energy of 1.2 mJ, the pulse repetition frequency of 1 kHz, and the initial beam diameter of 10 mm. The registration was performed using the second modification of the recording system [(*5b*) in Fig. 1].

Figure 7 shows the result of median filtering of the lidar signal spectrum in the altitude range 75–2000 m, averaged over

200 measurements. The measurements were performed with 30-minute acquisition time of the signal at the laser pulse repetition rate of 1 kHz. The inset in Fig. 7 shows the spectrum region in a scale enlarged along the ordinate axis, which corresponds to the Raman lines of nitrogen. After approximation of the elastic scattering peaks of the laser radiation and the Raman signal of nitrogen by means of the least squares method, we obtained the $I_{RS}$ ratio of the intensity of Raman scattering of nitrogen to the intensity $I_0$ of the peak relevant to elastic scattering of laser radiation. This ratio amounts to $5.6\times10^{-4}$, which is close to the literature data: according to [39], the ratio of cross sections of Raman scattering and elastic scattering is about $10^{-3}$.

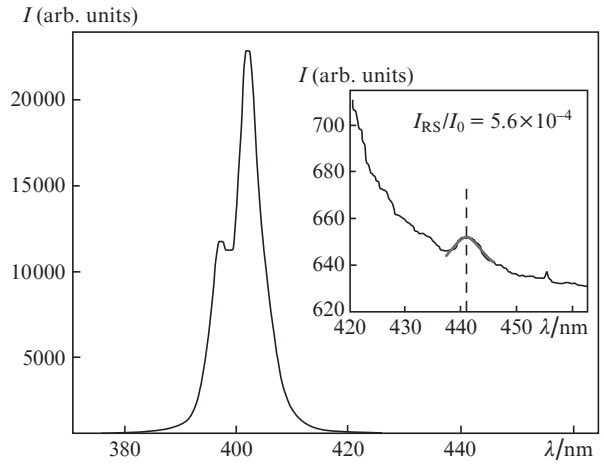


**Figure 7.** Lidar signal spectrum in the range of altitudes of 75–2000 m. In the inset shown is the spectrum region corresponding to the Raman line of nitrogen (the location of its maximum is indicated by the dashed vertical line).

## 9. Conclusions

As a result of the experiments on the atmospheric sensing using a femtosecond lidar with the pulses of gigawatt power, we have determined the possibilities for the research of gas and aerosol compositions of the atmosphere. It was established that:

1) for the configuration of the lidar system under consideration, the nonlinear effects occur in a 'dead' zone of the receiving system (at the distances up to 140 m), and then radiation propagates in the linear regime;

2) the results of sensing by means of the femto- and nanosecond lidars are in good agreement, which confirms the assumption on the linearity of propagation of the 'post-filamented' femtosecond radiation in the atmosphere;

3) the use of the developed device as a lidar of elastic scattering at the wavelength of 800 nm allows a signal to be reliably received at distances up to 11 km;

4) in the backscattered spectra of the sensing filamented femtosecond laser pulses with the centre wavelength of 800 nm, the emission lines of the first positive system of the nitrogen molecule $B^3\Pi_g - A^3\Sigma_u^+$ can be distinguished;

5) the use of the second harmonic of the Ti:sapphire femtosecond laser in the experiments allows registering the Raman scattering line for nitrogen ($\lambda \approx 441$ nm); the ratio of intensities of this line and the line of elastic scattering amounts to $5.6\times10^{-4}$ at the wavelength of 400 nm.

The results obtained and the emerging technique of the experiments on sensing the environment by high-power femtosecond lidars create a basis for the planned experiments at the IAO SB RAS, which assume the use a femtosecond atmospheric optical bench equipped with a system capable of generating the radiation pulses of terawatt power (with the energy of 100–150 mJ, duration of 50 fs and repetition rate of 10 Hz) of the fundamental and second harmonics of a Ti:sapphire laser (Avesta Project, Troitsk).

We should emphasise that the results of the experiments represent reliable evidence that the Russian researchers have attained the level of lidar sensing of the atmosphere with the use of the powerful ultrashort pulses.

***Acknowledgements.*** This work was supported by the Presidium of the Russian Academy of Sciences (Extreme Light Fields and Their Applications Programme), the integration project of the SB RAS – FEB RAS 'Development of Methods for Femtosecond Laser Sensing of The Atmosphere' and the Russian Foundation for Basic Research (Grant Nos 12-05-00716-a and 12-02 -31714_mol_a).

## References

1. Babin A.A., Kiselev A.M., Sergeev A.M., Stepanov A.N. *Kvantovaya Elektron.*, **31**, 623 (2001) [*Quantum Electron.*, **31**, 623 (2001)].
2. Apeksimov D.V., et al. *Femtosekundnaya atmosfernaya optika* (Femtosecond Atmospheric Optics) (Novosibirsk: Publishing House of SB RAS, 2010).
3. Geints Yu.E., Zemlyanov A.A., Kabanov A.M., Matvienko G.G. *Nelineinaya femtosekundnaya optika atmosfery* (Nonlinear Femtosecond Optics of The Atmosphere) (Tomsk: Publishing House of the Institute of Atmospheric Optics, SB RAS, 2010).
4. Il'yin A.A., Golik S.S. *Pis'ma Zh. Tekh. Fiz.*, **40** (1), 3 (2014).
5. Krekov G.M., Matvienko G.G. *Opt. Atmos. Okean.*, **23**, 835 (2010).
6. Bukin O.A., Pavlov A.N., Salyuk P.A., Golik S.S., Ilyin A.A., Bubnovskiy A.Y. *Opt. Atmos. Okean.*, **23**, 926 (2010).
7. Geints Yu.E., Kabanov A.M., Matvienko G.G., Oshlakov V.K., Zemlyanov A.A., Golik S.S., Bukin O.A. *Opt. Lett.*, **35**, 2717 (2010).
8. Geints Yu.E., Kabanov A.M., Zemlyanov A.A., Bykova E.E., Bukin O.A., Golik S.S. *Appl. Phys. Lett.*, **99**, 181114 (2011).
9. Geints Yu.E., Zemlyanov A.A., Kabanov A.M., Bykova E.E., Apeksimov D.V., Bukin O.A., Sokolova E.B., Golik S.S., Ilyin A.A. *Appl. Opt.*, **50**, 5291 (2011).
10. Golik S.S., Bukin O.A., Il'in A.A., Sokolova E.B., Kolesnikov A.V., Babiy M.Yu., Kul'chin Yu.N., Gal'chenko A.A. *J. Appl. Spectrosc.*, **79**, 471 (2012).
11. Geints Yu.E., Zemlyanov A.A. *Opt. Atmos. Okean.*, **23**, 749 (2010).
12. Geints Yu.E., Zemlyanov A.A. *Opt. Atmos. Okean.*, **23**, 757 (2010).
13. Ponomarev Yu.N., Uogintas S.R. *Opt. Atmos. Okean.*, **26**, 654 (2013).
14. Geints Yu.E., Zemlyanov A.A., Kabanov A.M., Matvienko G.G., Stepanov A.N. *Opt. Atmos. Okean.*, **22**, 119 (2009).
15. Zemlyanov A.A., Kabanov A.M., Matvienko G.G., Stepanov A.N., Bodrov S.B., Zakharov N.S., Kholod S.V. *Opt. Atmos. Okean.*, **22**, 332 (2009).
16. Apeksimov D.V., Bukin O.A., Bykova E.E., Heinz J.E., Golik S.S., Zemlyanov A.A., Zemlyanov Al.A., Il'yin A.A., Kabanov A.M., Matvienko G.G., Oshlakov V.K., Sokolova E.B. *Opt. Atmos. Okean.*, **23**, 536 (2010).
17. Apeksimov D.V., Geints Yu.E., Zemlyanov A.A., Kabanov A.M., Matvienko G.G., Oshlakov V.K., Stepanov A.N. *Opt. Atmos. Okean.*, **23**, 1006 (2010).
18. Bukin O.A., Bykova E.E., Heinz J.E., Golik S.S., Zemlyanov A.A., Il'yin A.A., Kabanov A.M., Matvienko G.G., Oshlakov V.K., Sokolova E.B. *Opt. Atmos. Okean.*, **24**, 351 (2011).

19. Kiselev A.M., Ponomarev Yu.N., Stepanov A.N., Tikhomirov A.B., Tikhomirov B.A. *Kvantovaya Elektron*., **41**, 976 (2011) [*Quantum Electron*., **41**, 976 (2011)].
20. Bukin O.A., Bykova E.E., Geints Yu.E., Golik S.S., Zemlyanov A.A., Il'yin A.A., Kabanov A.M., Matvienko G.G., Oshlakov V.K., Sokolova E.B., Khabibullin R.R. *Opt. Atmos. Okean*., **24**, 648 (2011).
21. Apeksimov D.V., Bukin O.A., Bykova E.E., Golik S.S., Zemlyanov A.A., Kabanov A.M., Matvienko G.G., Petrov A.V. *Opt. Atmos. Okean.*, **26**, 974 (2013).
22. Apeksimov D.V., Bukin O.A., Bykova E.E., Geints Yu.E., Golik S.S., Zemlyanov A.A., Kabanov A.M., Matvienko G.G. *Opt. Atmos. Okean*., **26**, 247 (2013).
23. Apeksimov D.V., Bukin O.A., Bykova E.E., Golik S.S., Zemlyanov A.A., Il'yin A.A., Kabanov A.M., Matvienko G.G., Oshlakov V.K., Petrov A.V., Sokolova E.B. *Opt. Atmos. Okean*., **26**, 1029 (2013).
24. Iglakova A.N., Matvienko G.G., Oshlakov V.K., Prokop'ev V.E., Timofeev V.I. *Opt. Atmos. Okean*., **26**, 969 (2013).
25. Woste L., Wedekind C., Wille H., Rairoux P., Stein B., Nikolov S., Werner Ch., Niedermeier S., Schillinger H., Sauerbrey R. *Laser und Optoelektronik*, **29**, 51 (1997).
26. Braun A., Korn G., Liu X., Du D., Squier J., Mourou G. *Opt. Lett.*, **20**, 73 (1995).
27. Méjean G., Kasparian J., Salmon E., Yu J., Wolf J.-P., Bourayou R., Sauerbrey R., Rodriguez M., Wöste L., Lehmann H., Stecklum B., Laux U., Eislöffel J., Scholz A., Hatzes A.P. *Appl. Phys. B*, **77**, 357 (2003).
28. La Fontaine B., Vidal F., Jiang Z., Chien C.Y., Comtois D., Desparois A., Johnson T.W., Kieffer J.-C., Pepin H. *Phys. Plasmas*, **6**, 1615 (1999).
29. *Publications of the Teramobile Project*; http://www.teramobile.org/publis.html.
30. Faye G., Kasparian J., Sauerbrey R. *Appl. Phys. B*, **73**, 157 (2001).
31. Gordienko V.M., Kholod A.I., Pryalkin V.I. *Kvantovaya Elektron*., **30**, 839 (2000) [*Quantum Electron*., **30**, 839 (2000)].
32. Marburger J.H. *Prog. Quantum Electron.*, **4**, 35 (1975).
33. Kandidov V.P., Golubtsov I.S., Kosarev O.G. *Kvantovaya Elektron*., **34**, 348 (2004) [*Quantum Electron*., **34**, 348 (2004)].
34. Kandidov V.P., Shlenov S.A., Kosarev O.G. *Kvantovaya Elektron*., **39**, 205 (2009) [*Quantum Electron*., **39**, 205 (2009)].
35. Kandidov V.P., Shlenov S.A., Silaeva E.P., Dergachov A.A. *Opt. Atmos. Okean*., **23**, 873 (2010).
36. Geints Yu.E., Zemlyanov A.A. *Opt. Atmos. Okean*., **23**, 274 (2010).
37. Geints Y.E., Bulygin A.D., Zemlyanov A.A. *Appl. Phys. B*, **107**, 243 (2012).
38. http://weather.uwyo.edu/upperair/sounding.html.
39. Zuev V.V., El'nikov A.V., Burlakov V.D. *Lazernoe zondirovanie srednei atmosfery* (Laser Sensing of The Middle Atmosphere) (Tomsk: RASCO, 2002).
40. Bukin O.A., Kulchin Y.N., Pavlov A.N., Stolyarchuk S.Y., Shmirko K.A. *Opt. Atmos. Okean*., **25**, 694 (2012).
41. Pavlov A.N., Shmirko K.A., Stolyarchuk S.Y. *Opt. Atmos. Okean*., **25**, 968 (2012).
42. Il'yin A.A., Bukin O.A., Sokolova E., Golik S.S., Shmirko K.A. *Opt. Atmos. Okean*., **25**, 441 (2012).
43. Ilyin A., Golik S. *Spectrochim. Acta*, *Part B*, **87**, 192 (2013).